ACE18 - AWWA Annual Conference & Exhibition
Las Vegas, Nevada
June 11-14, 2018

WATER MAIN BREAKS, WATER HAMMER. CORROSION, AND FATIGUE FAILURES

Robert A. Leishear, Ph.D., P.E., ASME Fellow
Leishear Engineering, LLC

ABSTRACT

Underground water main failures and subsequent leaks over the past century have been misdiagnosed or misunderstood as corrosion or unknown causes, where the actual failure causes were water hammers, which crack piping and also create localized crevices to cause corrosion and destroy piping. More than 250,000 water main breaks occur per year in the U.S. and Canada at a cost of a billion dollars per year, where one quarter of those failures are attributed to corrosion. That is, water hammer causes the piping cracks as well as most, if not all, of the corrosion failures. These failures can be prevented. Extensive studies of a generic fire protection water system and a coolant water system have proven this opinion.

Cast iron and ductile iron are used underground due to their high resistance to corrosion. However, piping corrodes and deteriorates at local "hot spots" due to pitting corrosion, where uniform corrosion is not observed over the entire surface of the piping in the vicinity of cracks.

Using present national piping code design requirements and previous technology, the cause of these piping failures could not have been identified at all. The studies presented here discuss recent developments in dynamic stress theory and how that theory is coupled with observed piping failures. The localized cracking of pipes due to water hammer provides fatigue cracks, which in turn provide localized areas to start corrosion inside the cracks and accelerate corrosion to fail the piping. Additionally concrete piping is known to crack, where water hammers cause these cracks as well. In other words, water hammer cracks nearly any type of piping, but corrosion increases leak sizes faster.

Typically, water hammer cracks are caused by pump operations, fire hydrant operations, and valve operations. Pump operations can be controlled by the utilities supplying water to their systems, while fire hydrant and user operations are more difficult to control. Even so, this technological breakthrough provides solution methods to resolve a costly, long-standing problem.

NOMENCLATURE

ASME American Society of Mechanical Engineers
AWWA American Water Works Association
DI ductile iron
MOC method of characteristics
NACE National Association of Corrosion Engineers
NPS nominal pipe size
NTSB National Transportation Safety Board
SRS Savannah River Site
WSAA Water Services Association of Australia

SYMBOLS (U.S. customary units are used throughout)

a wave speed in the liquid
a_1 a_2 a_3 wave speeds
A_1 A_2 A_3 pipe areas
D average pipe wall diameter
E modulus of elasticity
g gravitational constant.
k bulk modulus of the liquid
K fatigue limit reduction factor
Lv length of a pipe section filled with steam
Ls length of a propelled slug of water
P pressure applied to slug of liquid
P_i initial, or incident, pressure
P_r reflected wave
Ps pressure change due to a vapor collapse
P_t transmitted pressure
t wall thickness
Vs velocity of a slug of water
ΔP change in pressure due to a sudden valve closure
ΔV change in fluid velocity at the valve
$\Delta\sigma$ dynamic stress
ρ density
σ static load
v Poisson's ratio

INTRODUCTION

Piping failures pepper the engineering literature in almost every industry (Leishear [1 and 2]). For example, fatalities due to explosions of gasoline and anhydrous ammonia occurred at the time of valve operations and pump startups in pipelines (NTSB [3 and 4, respectively]), i.e., water hammer induced accidents. Also, thousands of other pipelines have ruptured during fluid transients, or water hammers. Outside the scope of this work, oil pipeline failures (estimated to be 7 billion dollar a year problem) are more complicated, where sludge deposits accelerate corrosion along the bottom invert of pipelines, and corrosive chemicals in solution

accelerate corrosion, but cracking caused by water hammer is also a contributor to many failures.

The sweeping scope of this problem cannot be addressed in a single study, but water hammer induced water main failures were investigated here as a major step toward an overarching understanding of underground piping failures, where underground piping failures occur in nearly all materials. This particular study clearly demonstrates the scale of this problem, where new theory was invented as required.

In other words, the primary goal of this work is not to criticize previous research, but to build on that research with new theory to understand water main failures with respect to water hammer. Consequently, this report uses previous research as a technical foundation.

This new theory can be summarized in half a dozen statements.

1. Pipes do not crack without a cause
2. Pipes do not fail because they are old.
3. Pipes crack due to fatigue or a sudden one-time overload failure, where fatigue is the common failure mode for operating systems.
4. Water hammer directly caused 69.5% of water main breaks, or cracks, in U.S. and Canadian piping, i.e., fatigue failures.
5. Water hammer also caused an additional 28.3% of water main failures in U.S. and Canadian piping, where corrosion accelerated piping failures were initially caused by cracks due to water hammer.
6. That is, corrosion is not the initiating pipe failure cause, water hammer is the primary failure cause followed by corrosion.

To present this theory, a literature review on water main failures is first considered, followed by discussions of fatigue, dynamic stress theory, water hammer, and corrosion. This collection of related theories is brought together by using pipe stress calculations for several simplified systems and an actual case study to provide proof of principle for the new theory presented here. Only a few examples are provided even though there are myriad system designs that are affected by water hammer or water hammer induced corrosion. Another primary goal of this work is to provide a foundation for future research in the area of underground pipeline failures.

LITERATURE REVIEW FOR WATER MAIN FAILURES

The literature is flooded with papers on water main and underground piping failures. However, several recent studies provide an excellent overview of the problem, even though water hammer was not known to be the primary failure cause at the time of those studies.

A Survey of Water Main Failures

In the first study, the University of Utah (Folkman [5]) performed a survey of water utilities that maintained an equivalent pipe length equal to 10% of the water main piping in the U.S. and Canada, which equaled 117,000 miles of pipe. A key question of the survey was related to the primary cause of piping failures experienced by each utility. The reported types of failures and types of materials are presented in Figs. 1 through 4, where metallic pipes are concrete lined. As shown in Figs. 1 and 2, cracks and fatigue are experienced in all types of piping and are reported to constitute 65.2% of water main failures. Leaks (4.3% of the failures) are caused by cracks, joint, or valve leaks, which are also caused by water hammer. Figures 3 and 4 indicate that pipe failures tend to increase with age and decrease with diameter, where both of these observations are consistent with fatigue failures, since smaller diameter piping frequently experiences higher pressures and higher hoop stresses.

Research presented here shows that pump, valve, and fire hydrant operations causes fatigue cracks in piping. Research also shows that water hammer is the cause leading to corrosion accelerated failures in piping (28.3% of the failures). That is, most, if not all, of the reported water main corrosion problems are caused by water hammer. In other words, approximately 97.8%, or more, of the U.S. and Canadian piping failures per year are due to water hammer - 244,500 piping failures per year are caused by water hammer, costing 978 million dollars per year in the U.S. and Canada alone.

Failure Modes in Water Main and Sewage Piping

In a second study, the Water Services Association of Australia (WSAA [6]) investigated underground water main and sewer services, where internal corrosion due to sewage was a failure mode in addition to water hammer. Figures 5 through 15 show the effects of cracking and corrosion on numerous materials.

Failure Modes in Large Diameter Water Mains

In a third study, 6181 piping failures were evaluated with a focus on corrosion as a cause, where dynamic stresses due to water hammer were not considered. Piping was primarily cast iron and steel concrete lined piping between in 95 and 280 inches in diameter.

Rajeev, et al [7] determined corrosion rates in this study, but most failures were associated with cracks, which is consistent with the theory promoted here. Some failures were attributed to pinhole leaks, which could only have occurred if the inner concrete pipe linings were cracked from water hammer. They noted that most failures occurred near the bell of pipes where stresses are higher due to localized stresses, and they also noted that traffic and external loading were considered to be contributing failure causes for small diameter pipes. In

other words, traffic on roads and steady state loads would contribute to fatigue damages from water hammer.

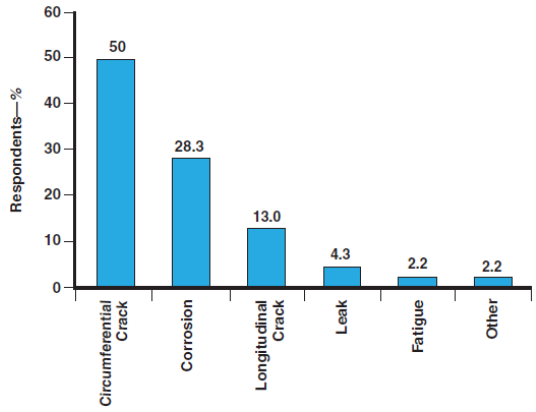

Figure 1: Types of Water Main Piping Failures (Folkman, et al, [5])

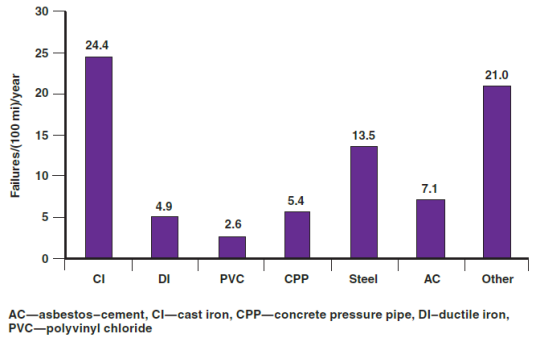

Figure 2: Failures for Different Materials (Folkman, et al, [5])

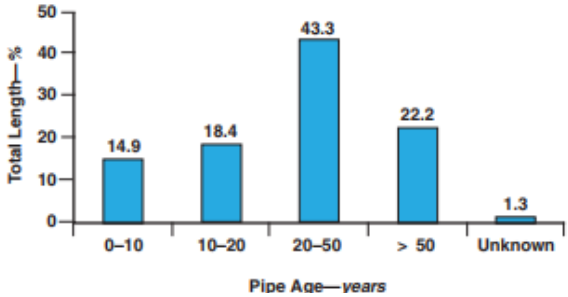

Figure 3: Failures for Different Pipe Ages (Folkman, et al, [5])

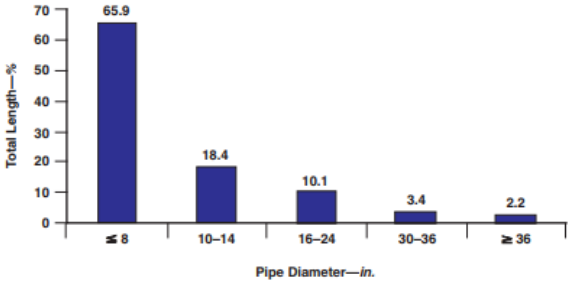

Figure 4: Failures for Different Pipe Diameters (Folkman, et al, [5])

Figure 5: Cast Iron Cracking and Corrosion (Figs. 5 – 15 Reprinted by permission, WSAA [6])

Figure 6: Cast Iron Cracking Without Corrosion (Figs. 6 – 15 reprinted by permission of WSAA [6])

Figure 7: Ductile Iron Cracking and Corrosion (WSAA [6])

Figure 8: Copper Cracking Without Corrosion (WSAA [6])

Figure 9: PVC Cracking (WSAA [6])

Figure 10: Copper Cracking and Corrosion (WSAA [6])

Figure 11: HDPE Electrofusion Joint Leakage (WSAA [6])

Figure 12: HDPE Butt Weld Crack (WSAA [6])

Figure 13: Cracks in Brass Elbows (WSAA [6])

Figure 14: Asbestos Cement Cracking (WSAA [6])

Figure 15: Corroded and Cracked Underground Valve (WSAA [6])

WATER HAMMER, DYNAMIC STRESS THEORY, AND FATIGUE FAILURES

Continuing the literature review, relationships between water hammer, dynamic stresses, and fatigue failures have been extensively documented, where the reader is referred to that work for details (Leishear [1 and 2]). In that work, new theory, referred to as the Dynamic Stress Theory, was developed to describe the pipe stresses that occur when pressure waves due to water hammer travel along the bore of a pipeline at near sonic velocities. That work is abbreviated here to background this research. Although numerous piping materials fail in water main service, consideration is limited here to steel, ductile iron (DI), and high density polyethylene (HDPE) to compare material effects on piping failures.

FATIGUE THEORY

The main conclusion of this evaluation is that fatigue due to water hammer is the primary failure mechanism for water mains, and accordingly a discussion of fatigue introduces this failure analysis. Water hammers contribute to fatigue cycling, where some hammers cause stresses to exceed fatigue limits. In short, many cyclic loads have been applied to water main systems, and fatigue is the cause of hundreds of thousands of previous piping failures, where water hammer causes cracks and corrosion that accelerates other pipe cracks. There are several relationships that relate fatigue limits to applied pressures and the number of cycles to failure, which are outside the scope of this work. Additional calculations are provided here to understand fatigue failures, along with the following fatigue discussion.

Fatigue occurs in structures due to cyclic loading, where a limiting lower stress typically defines the fatigue limit. For stresses below this limit, the endurance, or reliability, of a structure is typically assumed to be unlimited with respect to stress induced failures. Although recent research suggests that there is not a lower limit for fatigue at very high cycles for welded steel piping, fatigue limits will be used for analysis.

Iron and Steel Microstructures

Failure of irons and steels may be in the form of tensile straining (overload) of materials or fatigue cracking of materials, where fatigue is the primary focus of this study. The basic mechanism of fatigue is shown in Fig. 16, where small microstructural defects join together to form larger defects that finally join together to form planar cracks. To understand fatigue, first consider the general effects of microstructure on material properties with respect to failures of irons and steels.

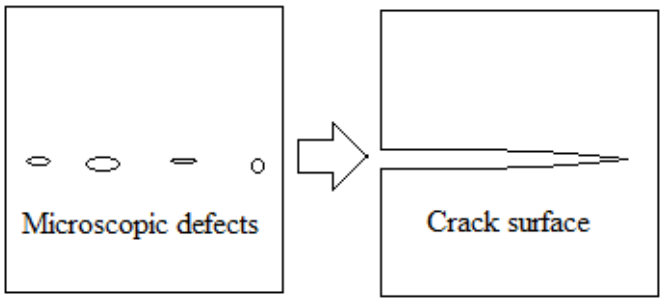

Figure 16: Fatigue Failure Mechanism (Note that the crack surfaces shown are formed by a crack growing inward from the edge of a part. See also Brooks and Choudry [8] to view photomicrographs of fracture surfaces and Andersen [9] for a detailed discussion of fracture mechanics)

The microstructures of metals consist of crystals, and the crystal strengths of iron and its alloys depend on lattice defects, which are atoms or empty spaces that occur in place of carbon or iron atoms in the lattice. The basic mechanism for yielding and tensile failure occurs due to motion along slip planes in the crystals to cause plastic deformation. Common crystal slip planes for cast iron, steel, and ductile iron are shown in Fig. 17, where steel, cast iron, and ductile iron are each a type of iron. At low temperatures, each of these materials has a body centered cubic (BCC) crystal lattice structure, as shown in Fig. 18, and the direction of the crystal slip planes can vary from one grain to the next. During microscopic plastic deformation, motion may occur along any slip plane of the BCC crystals as forces are applied[1]. During microscopic cracking, cracks form along these same planes. This type of cracking is referred to as transgranular, or through the grain, cracking, where cast iron is a brittle material that primarily fails due to transgranular fractures.

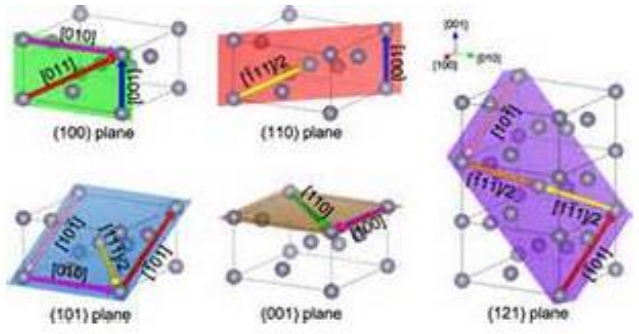

Figure 17: Slip Planes in BCC Crystals (Note that transgranular cracking may grow along any of the crystallographic planes without preference for a specific slip plane.)

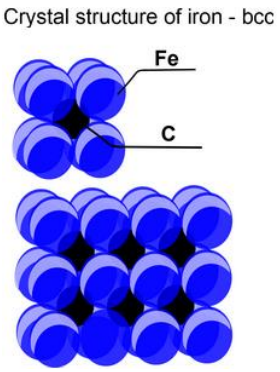

Figure 18: Body Centered Cubic Crystal Lattice Structure of Irons and Steels

Fatigue cracks in metals are also more complicated due to grain structures, where a typical steel grain structure is shown in Fig. 19. Steels are alloyed with materials such as Manganese to replace carbon atoms in the lattices and increase the strength of the steel, where irregularities (defects) in the slip planes affect microscopic cracks. That is, this strength increase of crystals inhibits fatigue crack growth along the slip planes in crystals. Additionally, carbon and impurities collect at grain boundaries, which are less resistant to cracks than crystals. Cracks then grow along the grain boundaries rather than through the body of the crystals, where this mechanism is known as intergranular fracture[2] (Fig. 20). Microscopic intergranular or transgranular crack surfaces can only be differentiated through microscopy and fractography and cannot be visually observed.

[1] The type of crack is further complicated during stress corrosion cracking, where metal cracks can be either intergranular or transgranular, depending on how the corrosion reactions occur in the crystals or grain boundaries.

[2] One method to inhibit cracking is to anneal steels by heating to merge the grains and align the lattices of the crystals to reduce grain boundaries.

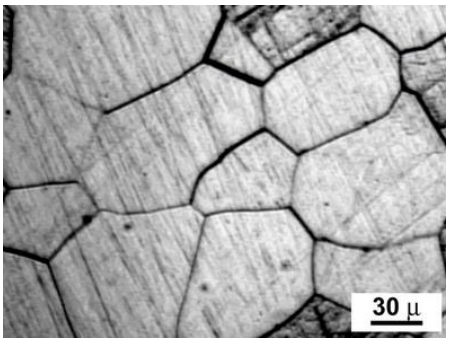

Figure 19: Typical Grain Structure in Steels
(pic2fly.com)

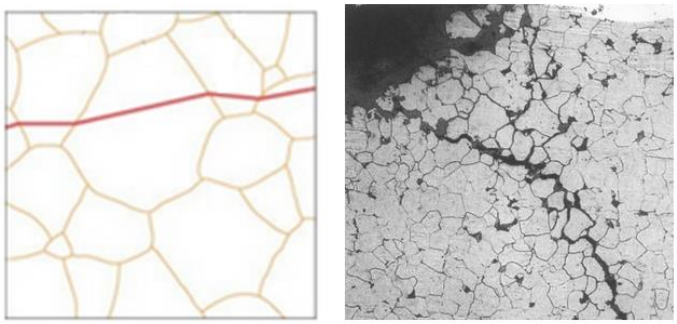

Figure 20: Types of Cracks in Irons and Steels
(products.asminternational.org. Reprinted by permission of the American Society of Metals)

Iron and Steel Macroscopic Fracture Surfaces

Visually, macroscopic crack surfaces depend on the tearing or ripping of metals to cause asperities on the crack surfaces. That is, crystal deformations will not be seen by the naked eye on the crack surfaces of pipes or components, where crack surfaces tend to reflect brittle or ductile failures.

In brittle cracks, rough fracture surfaces are grainy, and cracks tend to occur at right angles to the surfaces of pipes or components. In brittle fatigue fractures, cracks tend to occur along the principal planes as defined in Fig. 21, where cast iron is an example of a brittle fracture.

Ductile failures are more complicated, where these fractures sometimes initiate at 45 degree angles to the crack surface and have smooth ductile fracture surfaces along the crack faces for a short distance, where the maximum stresses to cause macroscopic cracks tend to occur on maximum shear planes as shown in Fig. 21. As a ductile crack propagates through a material, the fracture growth directions change from 45 degrees with respect to the crack surface to 90 degrees with respect to the crack surface. That is, the fracture mechanism changes from ductile to brittle. An interesting aspect to of this phenomenon is that ductile tearing frequently appears shiny as the asperities of the crack are smeared due to shear (Fig. 16), while the brittle fracture asperities stretch outward from the crack surface to form grainy surfaces on steels. Although photos are unavailable, cracks in an SRS cooling system pipe were inspected in the early 1990's, and a small, shiny section of ductile deformation was observed at the point where the crack initiated, where most of the through the circumference crack was a grainy surfaced brittle crack. In other words, the crack in the pipe started as a ductile fracture and sheared the pipe predominantly in a brittle manner, where there was very little plastic deformation or localized thinning of the pipe wall.

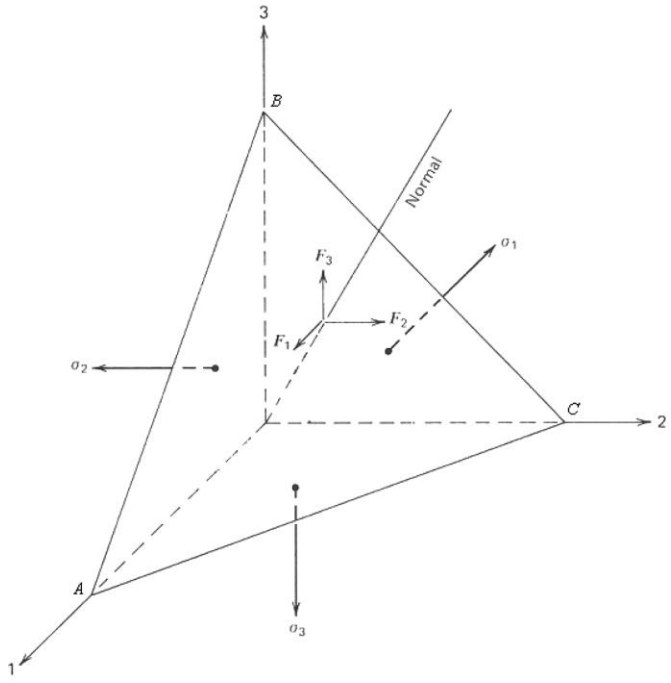

Figure 21: Maximum Shear Planes in Irons and Steels (Principal planes are the x, y, and z planes)

Ductile Iron Microstructures

Now consider ductile iron, where ductile iron pipe is a variation of manufactured iron pipe. The most significant impurities in the ductile iron are not in the form of lattice defects, but are in the form of graphite nodules, which inhibit bulk slip plane motion, and strengthen the ductile iron to significantly increase yield strengths and ultimate strengths above those of cast iron. The fatigue limit is directly related to the graphite nodules and the non-homogenous texture of ductile iron, where ductile iron has many initiation sites for cracks to start growing. In other words, the microstructures of encased graphite (Fig. 22) change iron from a brittle material that cracks with little yielding before failure to a ductile material that exhibits strain and yielding, or stretching, to the tensile strength before failure.

This effect is caused by the fact that the randomly distributed graphite nodules act as stress raisers, or pre-existing defects, or flaws, in the ductile iron

microstructure. The random distribution of the graphite nodules can induce failures anywhere in the pipe wall at any of the different size nodules or clusters of nodules. Accordingly, the literature reports a large spread in fatigue data for ductile iron, which implies that ductile iron is more likely to fail than over a wide range of cycles to failure. Also note that ductile iron has a higher tensile strength and lower fatigue limit than mild steel, A53, due to the nodular structure off ductile iron.

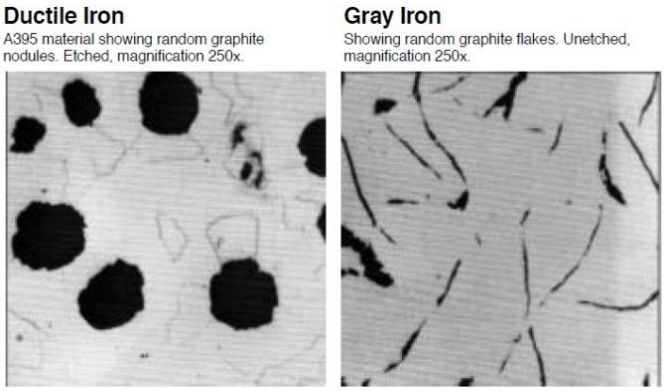

Figure 22: A395, Comparison of Ductile Iron (60-42-10) to Gray Cast Iron, Magnified 250X (https://www.flowserve.com/sites/default/files/2016-07/bulletin_A6.pdf, Reprinted by permission of Flowserve)

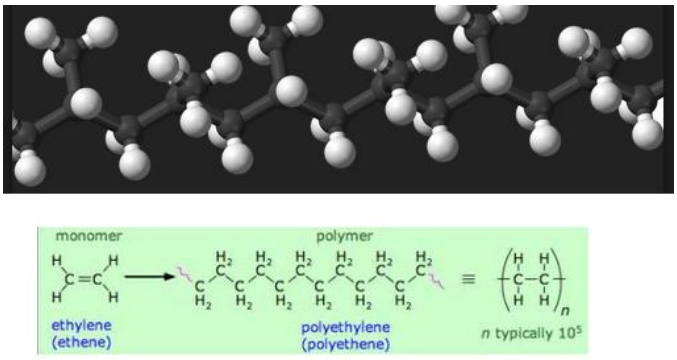

Figure 23: HDPE Molecule

HDPE Piping Microstructures

HDPE piping is resistant to corrosion, and the water hammer theory presented here explains HDPE failures. The microstructure of HDPE is far more complex than metals, where polymers, or chains, of molecules are dispersed throughout the material, where Fig. 23 shows the structure of an HDPE molecule. Fabrication and welding processes greatly complicate material properties, where Fig. 24 shows a theoretical distribution of polymers close to the surface of a material, and how they are stretched across a heated butt weld joint or fusion joint when two sections of pipe are fused, or welded together. In short, repeated water hammers cause failures of couplings and butt welds, and may result in failures elsewhere in HDPE piping. The fact that plastics and concrete failures are plentiful demonstrates the commonality of water hammer as a failure cause for may events.

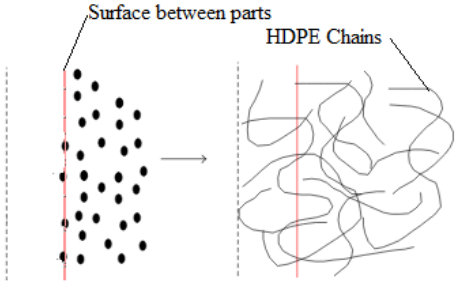

Figure 24: HDPE Microstructure

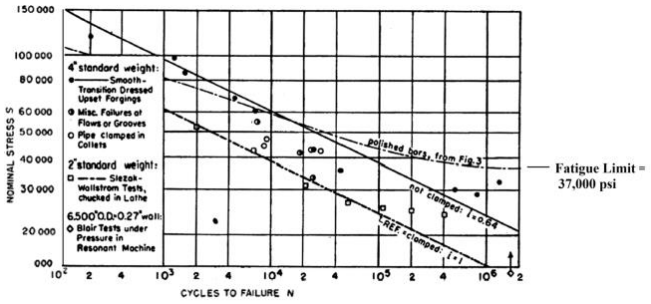

Figure 25: Fatigue Limits for 4" NPS, Schedule 40, Steel Piping (Markl [10])

PIPING FATIGUE DATA

Fatigue data from the literature are required to consider piping failures, where fatigue curves and fatigue limits generally define the average values obtained from experimental testing. The fatigue limit is affected by several factors, which include the material selection foremost. Fatigue curves for steel, HDPE, and ductile iron are provided here as references to better understand the failures of water main piping.

Note that the fatigue curve for steel (Fig. 25) shows that the fatigue limit for a polished bar test of steel piping equals 37,000 psi. Using the approximate fatigue correction factor shown in Fig. 26, the fatigue limit is estimated as

$$\text{Fatigue limit for steel} = 0.72 \cdot 37{,}000 \text{ psi} = 27{,}750 \text{ psi}. \quad (1)$$

Also note that the fatigue limit for bending of elbows is near 13,000 psi for through wall cracks (Markl [10]), where hoop stresses and bending stresses for elbows are assumed to behave differently. Consequently, the 27,750 psi estimate was referenced in calculations for this work.

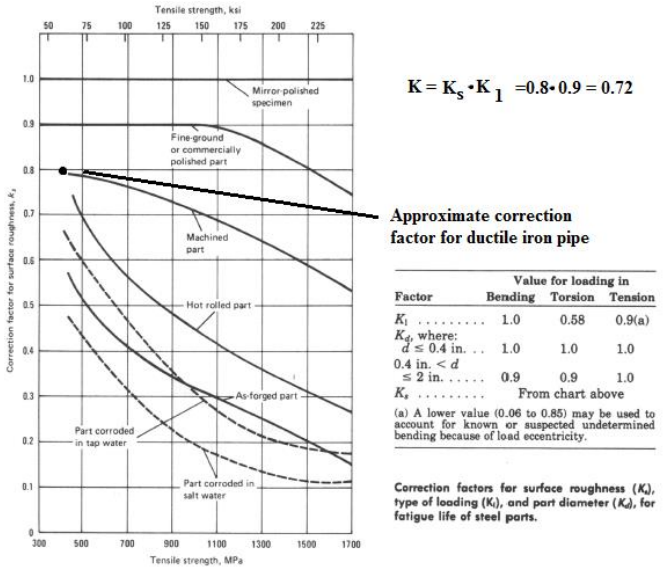

Figure 26: Fatigue Limit Correction Factor (ASM [11])

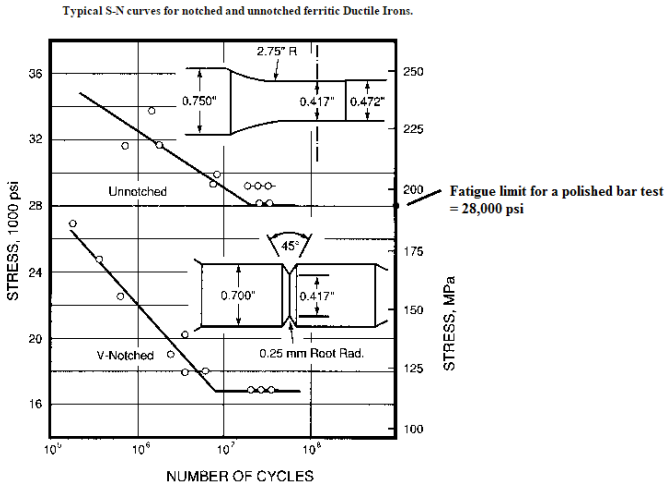

Figure 27: Fatigue Limit for Ductile Iron Piping (Adapted from DIS [12], Reprinted by permission of the Ductile Iron Society)

Note that the fatigue curve for ductile iron (Fig. 27) shows a fatigue limit of 28,000 psi, where this data was obtained for a polished bar test. Since ductile iron piping has a factory finish, the actual fatigue limit will be less than 28,000 psi, where a fatigue limit reduction factor, *K*, can be obtained from Fig. 10 as approximately 0.72. The fatigue limit for ductile iron is then estimated as

$$\text{Fatigue limit for ductile iron} = \\ = K \cdot 28{,}000 \text{ psi} = 0.72 \cdot 28{,}000 \text{ psi} \\ = 20160 \text{ psi}. \qquad (2)$$

Note that HDPE may not have a fatigue limit at all (Fig. 28), but a fatigue limit is assumed at 10^6 cycles, which is a common practice. The fatigue limit for HDPE is estimated from Fig. 28 as

$$\text{Fatigue limit for HDPE} = 1625 \text{ psi}. \qquad (3)$$

These fatigue limit values along with ultimate tensile strengths provide references for this work. Cyclic stresses cause fatigue, and ultimate strengths cause rupture.

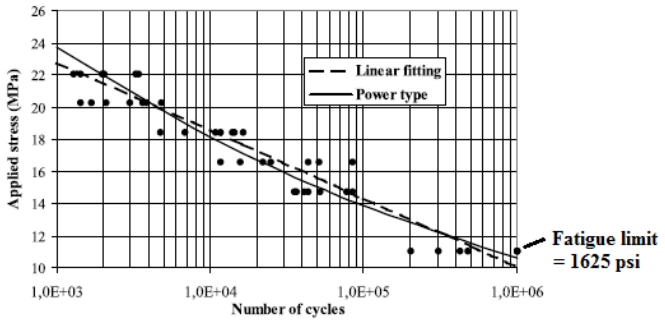

Figure 28: Fatigue Limit for HDPE Piping (Khelif, et al [13], Reprinted by permission of Springer Verlag, Inc.)

Fracture Mechanics

The principles of fracture mechanics provide a method to stop water hammer damages. There is a lower threshold stress below which a crack cannot grow (Collins [14]). If water hammer pressures are reduced to prevent any stresses from occurring below this threshold level, the crack cannot increase in size. That is, any cracks on the inside of the piping that have not reached the outer surface of the piping will not grow in size. However, cracks that have reached the outer surface will continue to grow in size due to pitting corrosion. In short, if a water hammer cause is stopped, the resultant cracks can be arrested as well, but cracks already started due to corrosion may continue to increase in size.

AN INTRODUCTION TO WATER HAMMER

Water hammer is a very complex process, and a simplified discussion of water hammer fundamentals is warranted. Some equations and graphs are presented to provide visualizations of the mathematics that pervades the rest of this report.

Pressure waves occur in piping systems when valves are opened or closed and pumps are started or stopped. That is, any change in flow rate is accompanied by pressure waves that transmit those flow rate changes and resultant pressure changes throughout the system. The transmitted pressure waves travel along the bore of the piping at velocities less than the sonic velocity, or acoustic velocity, of the fluid inside the piping. For simplicity of discussion, water hammer due to valve openings, pump operations, two phase flow and gas flow are not considered in detail here.

Pressure Wave Water Hammers

That is, there are many causes of water hammer pressure waves, but this analytical discussion is primarily restrained to only two causes, which are pertinent to this work. A primary cause of water hammer pressure waves in liquid filled systems – termed pressure wave water hammer in this work – arises from suddenly closed valves. A secondary cause considered here arises from reflected waves that occur subsequent to the initial pressure waves in pipe(s).

Water hammer equations can be expressed in terms of thin wall approximations or thick wall approximations. The thick wall equations provide increased accuracy, but the thin wall approximations are used here since they are reasonably accurate with respect to the uncertainty of the approximations used in this evaluation. Note that fluid flow calculations, and consequently water hammer calculations, generally only have an uncertainty within 20-30%. Additionally reflected wave and valve closure rates significantly affect approximations used in supporting calculations for this report. In short, several models were investigated to provide a general understanding of the effects of water hammer pressures on system piping and components.

Sudden Valve Closures

The change in pressure due to a sudden valve closure is expressed by

$$\Delta P = \frac{\rho \cdot a \cdot \Delta V}{g} \tag{4}$$

$$a = \sqrt{\frac{\frac{g \cdot k}{\rho}}{1 + \left(\frac{k}{E}\right) \cdot \left(\frac{D}{t}\right) \cdot \left(1 - \nu^2\right)}} \tag{5}$$

where ΔP is the change in pressure due to a sudden valve closure, ΔV is the change in fluid velocity at the valve, a is the wave speed in the liquid, k is the bulk modulus of the liquid, ρ is the density, E is the modulus of elasticity of the pipe wall, D is the average pipe wall diameter, t is the wall thickness, g is the gravitational constant, ν is Poisson's ratio, and the quantity $\left(1-\nu^2\right)$ reflects the conditions for a pipe restrained along its entire length, which is compatible with underground piping conditions.

Note that the maximum pressure described by Equation 4 is the pressure magnitude that is used for simplified calculations in this report with respect to valve closures. That is, the effects of valve closure times may significantly decrease predicted pressures obtained from this equation, where closure times are briefly discussed below.

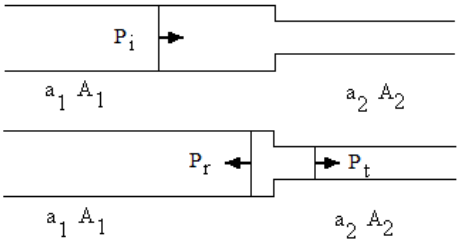

Figure 29: Pressure Waves at Reducers and Material Changes in Piping

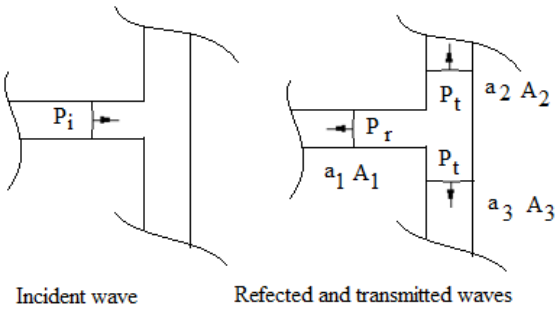

Figure 30: Pressure Waves at Tees

Reflected Pressure Waves at Reducers and Material Changes

To further complicate analyses, reflected waves occur at changes in diameter, changes in material, and at tees where the flow separates to go in two directions. An example that shows the effects of a change in material follows, where a change in diameter at a reducer would be similar but not identical. Note that reflected wave effects are only approximated herein for transient pressure magnitudes, where the predicted pressures may be different than the actual pressures in pipelines, where some reflected waves may be neglected due to approximations. When any fluid transient occurs, a pressure wave is initiated that travels throughout the piping system. At every reducer, tee, and change in material, reflected and transmitted waves are produced, where each of these waves will result in additional waves when they reach reducers, tees, and material changes. The maximum value of reflected wave pressure effects is twice the magnitude of the incident pressure, where pressures are doubled at closed ends (dead legs or dead ends) of piping when the wave reflects from the closed end of the pipe. Consequently, failures near the ends of pipelines are more likely.

The magnitudes of reflected pressure waves can be determined from the following equations.

$$P_t = P_i \cdot \frac{\frac{2 \cdot A_1}{a_1}}{\frac{A_1}{a_1} + \frac{A_2}{a_2}} \tag{6}$$

$$P_r = P_i \cdot \frac{\frac{A_1}{a_1} - \frac{A_2}{a_2}}{\frac{A_1}{a_1} + \frac{A_2}{a_2}} \quad (7)$$

where P_i is the magnitude of the initial, or incident, pressure, P_t is the transmitted pressure at the material or diameter transition, P_r is the reflected wave at the transition, A_1 and A_2 are the pipe areas, and a_1 and a_2 are the wave speeds, as shown in Fig. 29. Note that the wave speed Equation 5 is a function of both material properties and the pipe diameter. Consequently, wave speed changes (Equations 6 and 7) influence the pressure wave magnitudes of P_r and P_t.

Reflected pressure waves at tees

Pressure waves at tees are described by the following equations and Fig. 30. Note that the same pressure is transmitted to both downstream pipes.

$$P_t = P_i \cdot \frac{\frac{2 \cdot A_1}{a_1}}{\frac{A_1}{a_1} + \frac{A_2}{a_2} + \frac{A_3}{a_3}} \quad (8)$$

$$P_r = P_i \cdot \frac{\frac{A_1}{a_1} - \frac{A_2}{a_2} - \frac{A_3}{a_3}}{\frac{A_1}{a_1} + \frac{A_2}{a_2} + \frac{A_3}{a_3}} \quad (9)$$

where a_3 and A_3 are a wave speed and an area, respectively.

Note that calculations in this report use the equation for transmitted waves, P_t , to approximate pressures that cause piping failures. Since there are other reflected pressure waves, this approximation may be in error where pressures in an actual system may be higher, but estimates using these equations will provide substantial insight into whether or not water hammer causes fatigue failures of piping to create leaks. That is, the system dynamics are complex, but there will be at least a short span of time where the predicted pressure does in fact approximately equal the actual pressure in water main systems. Even so, pressures could potentially be doubled due to reflections at some locations. Computer simulations are mandatory to accurately model reflected pressures in complex systems.

DLF's

An extensive study of a steam condensate system water hammer was performed at SRS, where data is recorded in Table 1 below for comparison to other results. Details of that study of a two inch diameter NPS, stainless steel piping system are available (Leishear ([1 and 2]), but that study is summarized here to understand the effects of dynamic load factors (DLF's). In that study, experimental data was shown to be equivalent to mathematical derivations for pipe stresses, which were based on fourth order differential equations to describe the elastic response of a pipe to an applied water hammer wave traveling inside a pipe Consequently, DLF's were determined, where these factors are used to multiply static loads to approximate the maximum forces, strains and stresses that result due to the application of time varying loads. Specifically, the DLF equals the maximum dynamic stress divided by the stress that would occur if the stress was due to a statically applied load.

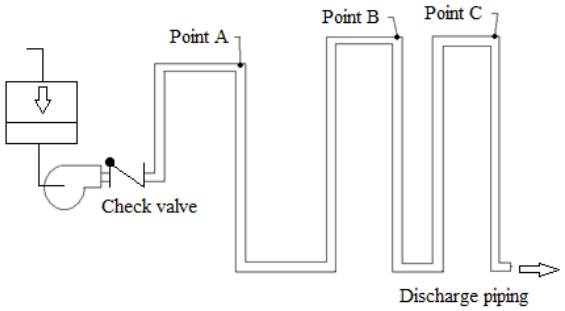

Figure 31: SRS, Vapor Collapse Investigation

Experimental validation of DLF's

For elastic hoop stresses, the maximum value of the DLF < 4. For bending stresses, the maximum DLF < 2 for a single elbow, where these DLF's may be multiplied, depending on the system geometry.

Noted DLF's are applicable to the initial pressure waves caused by a suddenly close valve, as described by Eq. 4. Detailed analysis may be performed to find the exact value of the DLF, but a

$$\text{DLF} < 4 \quad (10)$$

at the travelling wave was used for this analysis. That is the DLF < 4 at the wave, but reflected wave effects may increase the effective DLF. Also note that the DLF will be reduced to a DLF ≈ 1 during plastic deformation, which is outside the scope of this report.

Although much research has been completed to date, one set of experimental tests performed at Savanah River Site (SRS) will be briefly presented here to provide a better understanding of vapor collapse. The investigated system is shown in Fig. 31.

When the pump was shut down, water exited the discharge piping, and vapor spaces formed at points A, B, and C. The volume of those vapor spaces was determined by measuring the water level in the piping at point A. When the pump restarted, the vapor spaces collapsed as shown in Fig. 32, and pressure waves were transmitted through the piping, as shown in Fig. 33,

where the waves traveled near the calculated wave speed, *a*. The 590 to 925 psig measured pressures were within 30% of the pressures predicted from Eq. 11, which describes the pressure surge due to a vapor collapse (Green [15]).

$$Vs = \sqrt{\frac{2 \cdot Lv \cdot P \cdot g}{\rho \cdot Ls}} \tag{11}$$

$$Ps = \rho \cdot a \cdot \frac{Vs}{2 \cdot g} \tag{12}$$

where, *P* is an applied pressure, *Ps* is the pressure change due to a vapor collapse, *Lv* is the length of a pipe section filled with steam, *Vs* is the velocity of a slug of water, *Ls* is the length of a propelled slug of water, and *g* is the gravitational constant.

Water level in a horizontal 2" diameter pipe prior to water hammer

Water level in a horizontal 2" diameter pipe after water hammer

Figure 32: SRS, Void Measurements during Vapor Collapse

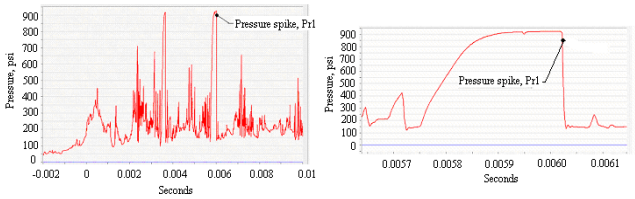

Figure 33: SRS, Pressure Measurements during Void Collapse

Also, a Bourdon tube pressure gauge indicated pressure surges of approximately 35 psi in this system, which had a 22 psig design pressure. Conclusively, slow response equipment like pressure gauges, check valves, and relief valves do not respond immediately to vapor collapse. However, in some valve closure cases, the pressure transients last long enough for relief valves to open during the second pressure wave transit.

Strains were measured in the piping (See Fig. 34), where strains are proportional to stresses. The DLF is less than 4 at the pressure wave; where a calculated DLF was within 30% of the measured DLF. To get this accuracy from differential equations, damping was considered where damping was not considered for the approximate analyses presented here. These water hammers were eliminated by installing a variable frequency drive on the condensate pump, where the linear startup time for the pump was set at 3 minutes as experimentally determined.

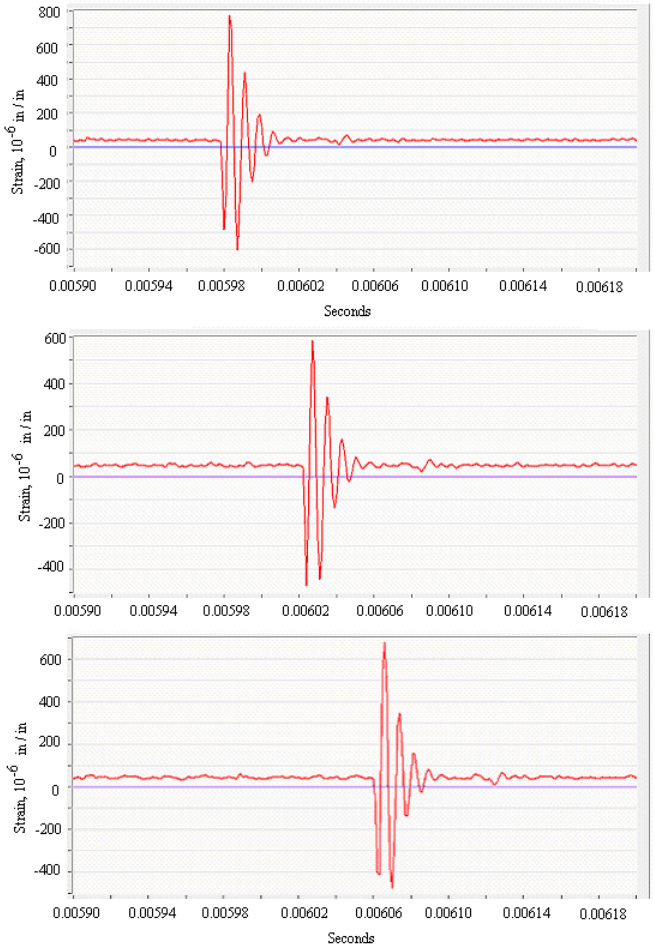

Figure 34: SRS, Measured Strain Waves during Vapor Collapse (The motion of a strain wave along the pipe wall was observed)

Hoop Stress DLF's For Reflected Pressure Waves

For water hammer reflected waves, the maximum DLF is expected to be less than 5, in the wake of vibrations that occur due to the shock waves in the liquid. The first vibration will be completely damped where the DLF ≈ 1, and when the reflected wave returns, the DLF < 4. Then, the total DLF equals 5. Consequently the DLF changes from 4 to 5 when reflected waves are considered at a piping dead end, which implies that the errors from neglecting reflected pressure waves equal 20 % for pressure wave water hammers. That is, the DLF's due to reflected waves during pressure wave water hammers are less than

$$DLF < 5 \tag{13}$$

For vapor collapse water hammers, the reflected

wave will have no effect on the DLF's. When the wave returns to any point along the pipe, the pressure will have returned to the operating pressure by that time, and the DLF never exceeds 4. The only locations in the system where reflected waves and incident waves may combine occur at dead ends. For reasons outside the scope of this paper, the DLF due to pressure wave at the dead end will not equal 4, where the DLF→2 at that dead end for a distance less than a foot or two from a dead end, reducer, or closed valve.

In short, reflected waves increase the potential for fatigue failures The effects of reflected waves on pipe stress calculation increase predicted pressures by less than 20% for pressure wave water hammers, and do not change the predicted pressures for vapor collapse water hammers.

Hoop Stresses

Having determined appropriate DLF's, the equations to describe dynamic hoop stresses are required. Consistent with this calculation, the thin wall approximation for hoop stresses, σ, is used, where the change in hoop stress due to a sudden pressure increase from a water hammer wave equals

$$\Delta\sigma = DLF \cdot \frac{\Delta P \cdot r}{t} = DLF \cdot \frac{\Delta P \cdot D}{2 \cdot t} \tag{14}$$

where the static hoop stress equals

$$\sigma = \frac{\Delta P \cdot r}{t} = \frac{\Delta P \cdot D}{2 \cdot t} \tag{15}$$

where $\Delta\sigma$ equals a dynamic stress, σ, equals the stress for a statically applied load, as described by Eq. 4.

Although not used in this analysis, the thick wall approximations for hoop stresses provide insight into actual piping failures. The fact is that cracks typically start at the inside surface of the piping where higher stresses occur, and cracks then grow toward the outer surface, unless the crack is initiated by a stress raiser near the outer surface, which initiates a crack such as a graphite nodule in ductile iron wall. The stress on the inner pipe wall is expressed as

$$\sigma_{inside} = \frac{P \cdot \left(OD^2 + ID^2\right)}{\left(OD^2 - ID^2\right)} \tag{16}$$

The stress on the outer pipe wall is expressed as

$$\sigma_{ouside} = \frac{P \cdot 2 \cdot ID^2}{\left(OD^2 - ID^2\right)} \tag{17}$$

where σ_{inside} is the static stress on the inner wall, σ_{inside} is the static stress on the outer wall, *ID* is the inner pipe diameter, and *OD* is the outer pipe diameter.

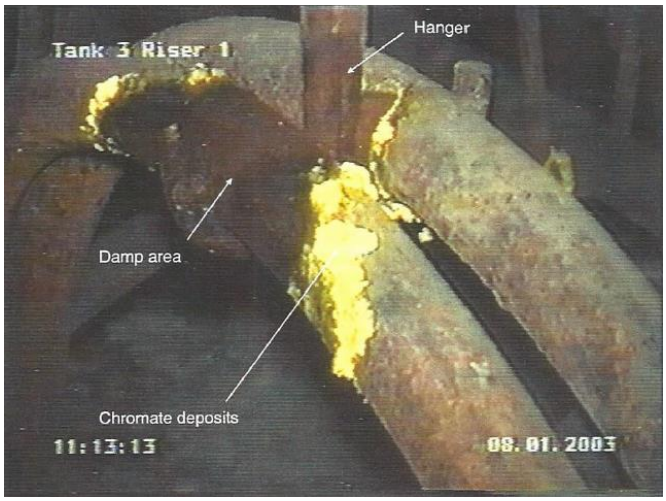

Figure 35: Typical SRS Cooling Coil Failure (Note that there is no significant local plastic deformation or localized thinning at the leak site)

A FATIGUE FAILURE ANALYSIS

Sufficient, but limited analyses were performed at SRS to explain piping failures where several conclusive results were obtained.

1. All piping cracks were preceded by valve packing leaks.
2. More than 200, two inch nominal pipe size (NPS), steel cooling coils cracked over 40 years inside radioactive liquid waste storage tanks, where localized stresses contributed to water hammer (See Fig. 35).
3. A dozen underground 6 inch and 8 inch NPS ductile iron pipes cracked through the circumference of the pipes.
4. All leaks occurred at the same time that water hammer events occurred, as documented in facility records.
5. An estimated 15 million dollar cost savings was realized from corrective actions that eliminated pipe system leaks.

A forty year history of unresolved piping failures was followed by new theory that is the foundation of this work. Cooling coil failures were inaccessible due to radiation in the tanks, and the cooling coil failures were attributed to corrosion for decades, until ductile iron piping failures started to occur. When ductile iron pipes were excavated for repairs, the pipes were observed to be sheared, and there was negligible corrosion on the fracture surfaces since the clay soil had low resistivity. Using the ASME B31.3 Piping Code, the conclusion was that the design was acceptable and piping could not fail, where static loads were assumed. A new theory was

invented to solve this problem over several years, and was called the dynamic stress theory, where dynamic load factors (DLF's) were used to prove that water hammer damaged all of the piping. This new theory was invented as damages occurred, but was, as yet, unproven. Consequently, damages were not immediately stopped.

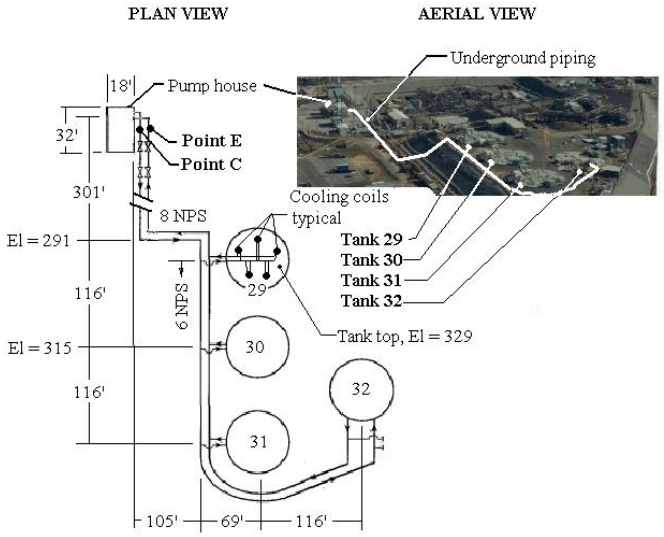

Figure 36: Modeled SRS System for Fatigue Failures Due to Water Hammer (approximately one million gallon tanks , 4 of 48 tanks shown)

There were four separate, but similar, cooling water systems. To model these systems and determine corrective actions, a widely accepted water hammer calculation technique, known as the method of characteristics (MOC), was used to calculate pipe stresses for part of one of the systems, and the other system was modeled by using similarity techniques. The modeled system is shown in Fig. 36. Figures 37 to 40 provide some of the fluid transient pressure results, where the reader is referred to Leishear [1 and 2] for detailed discussions. Piping stresses were calculated, as listed in Table 1 for the SRS, In-service Pump House and the SRS, Out of Service Pump House, where pipe stresses exceeded fatigue limits.

These two systems were combined by eliminating the Out of service pump house, and systems were also modified to reduce system water hammer pressures. Corrective actions (automatic slow closure rates for valves and check valves) eliminated all piping failures in these two systems for the past fifteen years except in two cases when corrective actions failed.

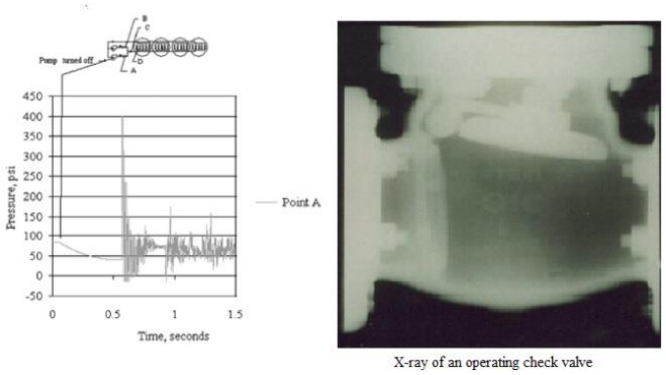

Figure 371: SRS, Pressures Due to a Check Valve Slam When Stopping One of Two Pumps

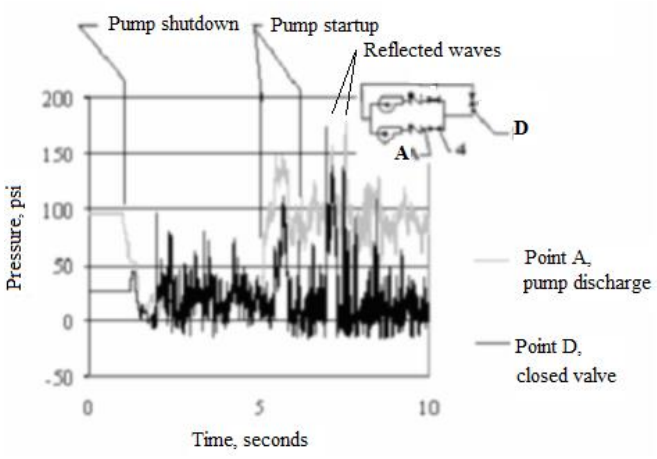

Figure 38: SRS, Pump Startup against a Closed Valve (Note that pump pressures nearly double during startups)

The other two systems were not modified due to cost considerations. The unmodified systems were severely damaged by water hammer, where the replacement system that was installed cost approximately five million dollars. That is, the new dynamic stress theory was expensively proven. Recommended water hammer pressure reductions methods were then implemented in the unmodified systems as well.

In short, water hammer corrective actions were implemented, and forty years of piping damages stopped. This success story is documented in a series of ASME papers that culminated in an ASME book, which included the failure analysis for these two hundred piping failures, along with the failure analysis of other piping damages and all of the pertinent theory to support that theory. Conclusively, this theory has been proven, and was published in its entirety in 2013 (Leishear [1 and 2]), where this dynamic stress theory is the foundation for the work performed here, along with additional new discoveries documented in this work.

Table 1: Maximum Pipe Stresses for Cooling System Piping and Condensate System Piping

The most significant table entries are highlighted as follows: Fatigue limits, Pipe stresses above the fatigue limits. Pipe stresses below the fatigue limit.

	8" NPS Ductile Iron, Initial Pressure and ΔP, psi	8" NPS Ductile Iron, Dynamic Bending Stress, psi	8" NPS Ductile Iron, Dynamic Hoop Stress, psi	8" NPS Ductile Iron, Combined Stress, 12 Failures, psi	8" NPS Ductile Iron, Fatigue Limit (Eq. 1), psi	2" NPS Ductile Iron, Initial Pressure and ΔP, psi	Coolant Coil, Dynamic Hoop Stress, psi	Coolant Coil, Constant Static Bending Stress, psi	Coolant Coil, Total Stress, 200 Failures, psi	2" NPS Carbon Steel, Fatigue Limit (Eq. 2), psi
SRS, In Service Pump House, 510 gpm (Fig. 39)	77, 200	-9000 min. 5250 max.	20628 max.	-9000 min. 21285 max.	20160	90, 1080	28531	4300	28853	27750
SRS, Out of Service Pump House, 1000 gpm	77, 200	-9000 min. 5250 max.	40447 max.	-9000 min. 45706 max.	20160	90, 1080	28531	4300	28853	27750

	Pressure Change ΔP, psi	2" NPS Stainless Steel, Static Stress, psi	2" NPS Stainless Steel, Maximum Actual Stress, DLF=3.86	2" NPS Stainless Steel, Minimum Actual Stress, DLF=2.87	2" NPS Stainless Steel, Thin Wall Stress, DLF=4	2" NPS Stainless Steel, Thick Wall Stress, DLF=4	2" NPS Stainless Steel, Approximate Fatigue Limit, psi
SRS, Condensate System	925	5777	22588	16308	24308	23109	32856

Notes:

1. Fatigue limit estimates for steel may be high, where approximations were made from Markl polished bar data, which is the basis was corrected for size and surface finish. Using B31.3, in-process fatigue data would yield lower failure limits.
2. For the Condensate System, the Markl fatigue limit estimate seems more realistic since the use of Section VIII values conservatively predict that there will be certain failure even though there were no observed failures, while the Markl values provide a better estimate for the range of the number of cycles and stress to cause failure.
3. Essentially, The Boiler and Pressure Vessel fatigue curves ensure safety for a 1% probability of failure, while the Markl fatigue curve provides the average values for fatigue at a 50 % probability of failure (See Fig. 41).
4. Data provided in ASME, Section VIII Fatigue Curves indicates that fatigue limits for carbon steel and stainless steel equal 12500 psi and 14800 psi respectively. Accordingly, the fatigue limit for stainless steel listed in Table 1 is approximately 18.4% higher than the carbon steel fatigue limit of Eq. 2 (See Leishear [1 and 2]).
5. For the Cooling System, ductile iron cracking started after the Out of Service Pump House was first placed in operation. Note that a very high number of cycles would be required for the Markl fatigue limit criteria, where the systems failed after 20 years of service and an unknown number of cycles.
6. Further research is recommended for fatigue cycling due to pressure pulsations, even though hoop stress fatigue limits are comparable to bending fatigue limits as determined by Markl and supporting research for ASME B31.3.
7. Cooling System calculations for the Out of Service Pump House were performed using similarity relationships based on flow rates and compared to Markyl fatigue data (Eq. 2).
8. Numerous calculations were performed using the MOC for the Cooling System, but only the maximum stresses from many different water hammer events are listed.
9. Note that the use of a DLF=1 yields erroneous predictions that failures will not occur for any conditions listed in Table 1, where corrective actions stopped all water hammers.
10. The effects of valve closure times depend on the length of the piping and materials A 10 second closure time may be slow for one system as in Fig. 40, but the same closure speed may act as a sudden valve closure in much longer systems. In fact, a pump may act as a suddenly closed valve in long piping systems.

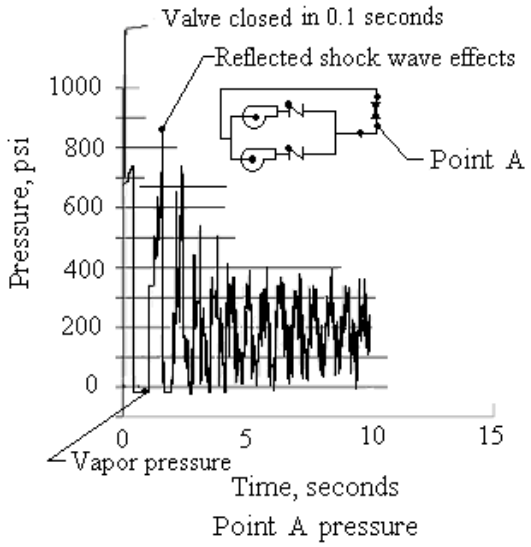

Figure 39: SRS, Cooling Coil Pressures Due to a Sudden Valve Closure (277 psi, Maximum Underground, Ductile Iron Piping Pressure. Note that the DLF < 4 for this suddenly applied load)

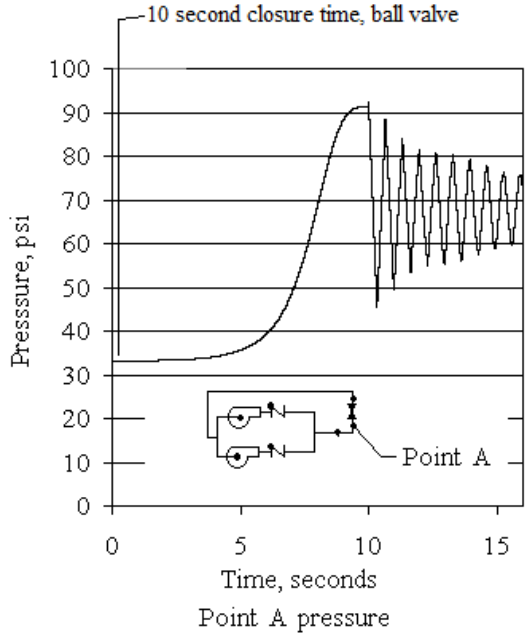

Figure 40: Pressure Changes in Cooling Coils Due to a Slow Closing Valve (This model is identical to Fig. 39, except for a linear, 10 second, slow valve closure speed. Note that the DLF = 1 for this slowly applied load).

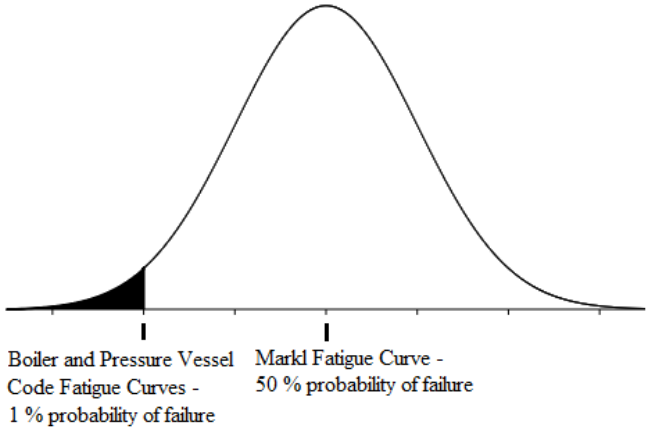

Figure 41: Comparison of Fatigue Curve Probabilities (Note that the number of cycles to fatigue failure typically varies by a factor of ± 10, or more)

EXAMPLES OF FATIGUE FAILURE STRESSES IN WATER MAINS

There are innumerable different water hammers in water mains, and examples of hypothetical fire hydrants are considered here to understand water hammer effects, where annual testing of fire hydrants is common (Fig. 42). Similar water hammers can be expected when industrial and commercial water users operate their facility water systems, where water hammer pressures can be much larger than those considered here. The goal of these calculations is to provide proof of principle for the theory that water hammer is the primary cause of water main failures.

Figure 42: Annual Fire Hydrant Testing

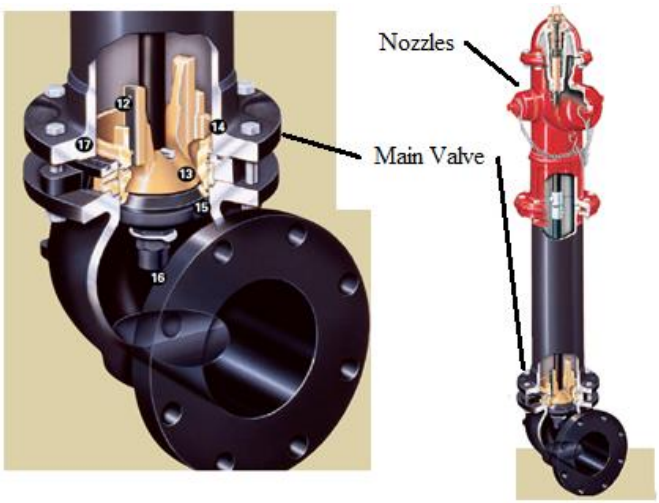

Figure 43: Fire Hydrant Installation with a Riser and an Underground Main Valve

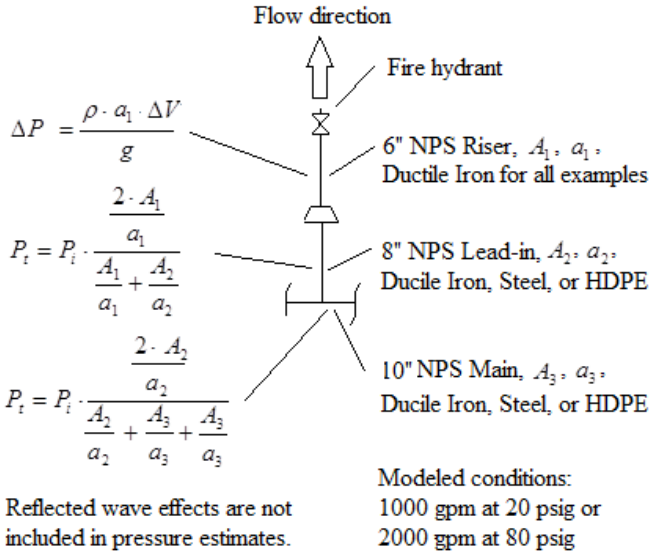

Figure 44: Simplified Water Main and Fire Hydrant Models

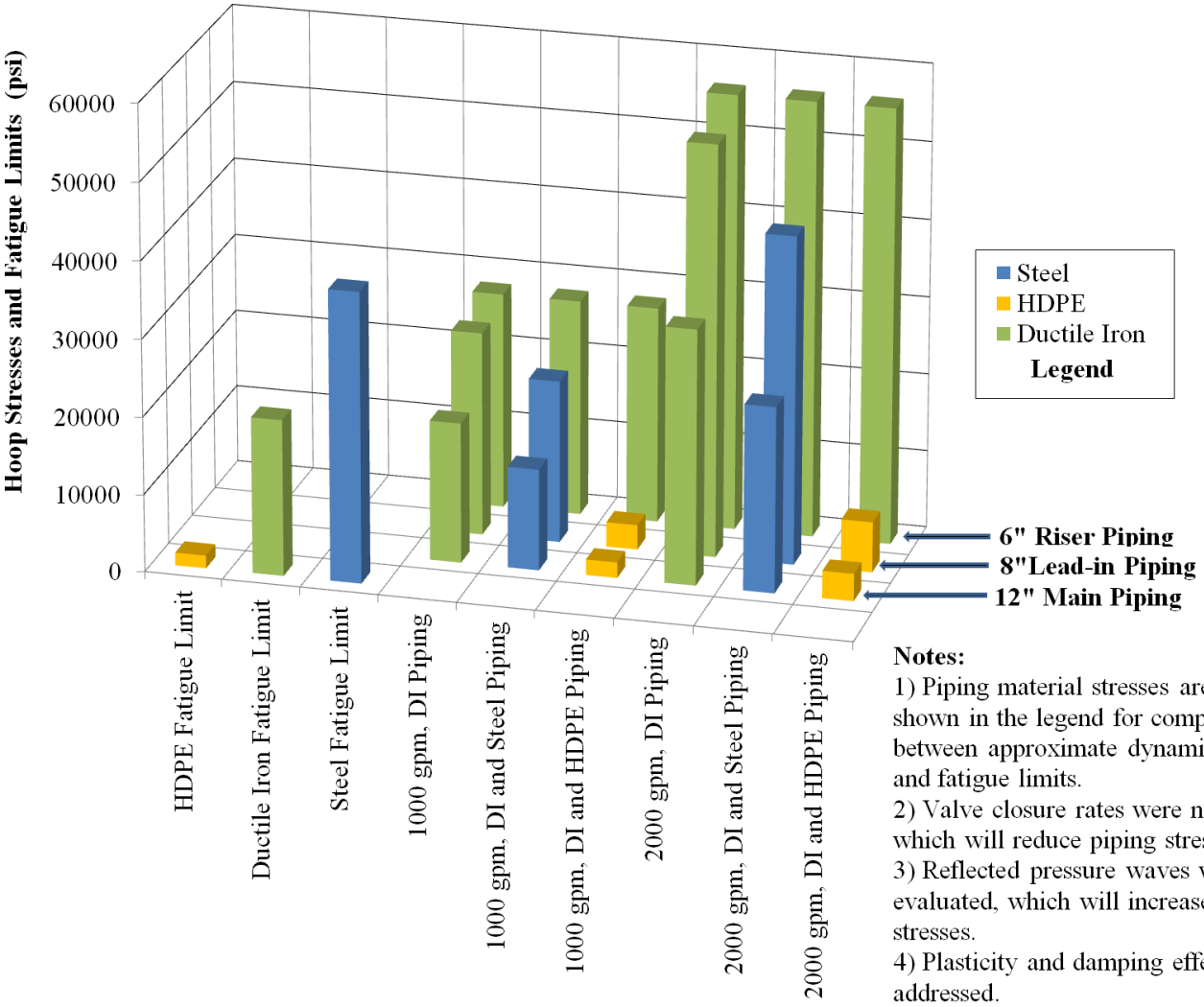

Notes:
1) Piping material stresses are color coded as shown in the legend for comparisons between approximate dynamic hoop stresses and fatigue limits.
2) Valve closure rates were not evaluated, which will reduce piping stresses.
3) Reflected pressure waves were not evaluated, which will increase dynamic stresses.
4) Plasticity and damping effects were not addressed.

Figure 45: Water Main Calculation Results

Water Main and Fire Hydrant Models

Terminology for these calculations is as follows. Risers are the vertical piping connected to the fire hydrants. Mains are the headers connected by lead-ins to the risers.

Although fire hydrant flows are governed by the nozzle diameters (and resultant frictional losses) that connect to fire hoses and equipment, a six inch valve and riser is assumed for approximations. Using this assumption, the lead-in and main piping diameters and materials are varied to compare different results. Piping material properties and dimensions were obtained from the Ductile Iron Society [10], AWWA [16], ASME [17], and ASTM [18 and 19]. Evaluated materials included Class 350, ductile iron, Schedule 40 A53, Grade A, ERW, steel, and DR9 HDPE.

The basic model is shown in Fig. 41, where Eqs. 1 through 6, 8, 13, and 14 were used as required on the figure, i.e., thin wall approximations were used without wave reflections to approximate pressures. Although numerous reflected waves occur in each pipe section, only a single reflected wave is considered in this approximate analysis. Accordingly estimated pressures will be lower than actual pressures in the risers and lead-in piping. Also, reflected waves from elsewhere in the system can increase pressures in the mains as well. Two flow rates are assumed for this analysis. The first flow rate is 1000 gpm, which is used by some municipalities as the minimum permissible hydrant flow when the system pressure drops to 20 psig. The second flow rate is 2000 gpm, which is the flow rate that would be provided for the same piping design for an 80 psig system pressure, where municipal water supplies commonly provide water pressures between 70 and 80 psig. Higher flow rates for other design conditions may be possible but were not evaluated. Sudden main valve closures are assumed, although hydrant closure times may be on the order of 15 seconds. Note that nozzle closures may act as sudden or slow valve closures, depending on the system pipe length and material of construction, where an evaluation of slow closure times is outside the scope of this work. Again, proof of principle is the intent here, where future research is recommended to investigate water main system complexities.

Water Main and Fire Hydrant Calculation Results

In short, water main cracks due to fire hydrant operations are caused by water hammer, where graphic results are displayed in Fig. 45. Fatigue damages are clearly evident for these smaller diameter pipes, where large diameter pipe failures will be comparable when valves and pumps are operated in the larger main piping. Again the intent of this work is to establish proof of principle as a guide for future research. This fundamental research will lead to better understanding of all underground piping failures.

CORROSION MECHANISMS

Having demonstrated that water hammer alone is the cause of many water main failures, the relationship between water hammer and corrosion deserves some exploration to investigate other failures. There are numerous types of corrosion discussed here, where these various corrosion mechanisms are closely related. As noted, water main failures are attributed to corrosion. In these failures, corrosion occurs in localized areas, where generalized corrosion over long lengths of piping surfaces are not typically observed as shown in Figs. 5 through 15. To explain the specificity of this corrosion, corrosion mechanisms need discussion.

As reported in the literature, anomalies in the piping surfaces are required to initiate corrosion, and moisture is also required. However, this work differs substantially from the literature, which concluded that corrosion was the primary cause of piping failures.

For the present theory, water hammer cracks provide the anomalies to start corrosion, where water then seeps from a water hammer crack to complete the corrosion processes. In other words, there is no doubt that water hammer causes cracking and resultant corrosion in underground steel, cast iron, and ductile iron piping.

Galvanic Corrosion

First consider "galvanic corrosion (also called dissimilar metal corrosion') which refers to corrosion damage induced when two dissimilar materials are coupled in a corrosive electrolyte. It occurs when two (or more) dissimilar metals are brought into electrical contact under water. When a galvanic couple forms, one of the metals in the couple becomes the anode and corrodes faster than it would all by itself, while the other becomes the cathode and corrodes slower than it would alone. The driving force for corrosion is a potential difference between the different materials" (NACE [20]). In some cases, sacrificial anodes are buried near piping to prevent piping corrosion but are frequently not installed for water mains.

Crevice Corrosion

Once the piping is cracked, low flow rates provide moisture to cause corrosion and a reasonably stagnant environment to augment crevice corrosion. "Crevice corrosion is a localized form of corrosion usually associated with a stagnant solution on the micro-environmental level. Such stagnant microenvironments tend to occur in crevices, where conditions deplete oxygen in the crevice and shift the crevice environment to acid conditions. As oxygen diffusion into the crevice is restricted, a differential aeration cell tends to be set up between crevice (microenvironment) and the external

surface (bulk environment). The chronology of the aggravating factors leading to a full blown crevice is shown in Fig. 46. Initially, oxygen content in the water occupying a crevice is equal to the level of soluble oxygen and is the same everywhere. The cathodic oxygen reduction reaction cannot be sustained in the crevice area, giving it an anodic character in the concentration cell. This anodic imbalance can lead to the creation of highly corrosive micro-environmental conditions in the crevice, conducive to further metal dissolution. This results in the formation of an acidic micro-environment…. Metal ions produced by the anodic corrosion reaction readily hydrolyze giving off protons (acid) and forming corrosion products. All forms of concentration cell corrosion can be very aggressive, and all result from environmental differences at the surface of a metal" (NACE [21]).

Together, the principles of galvanic corrosion and crevice corrosion provide an explanation for incipient localized corrosion of water main piping. Galvanic corrosion with acidic soils is the driving process, and crevice corrosion localizes that process.

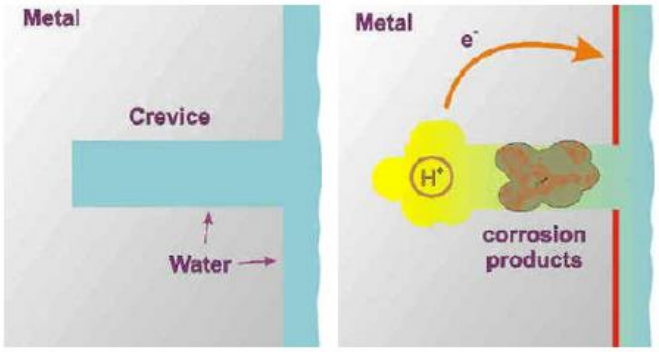

Figure 46: Crevice Corrosion (NACE [21])

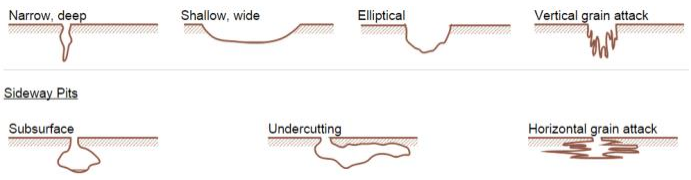

Figure 47: Types of Pitting Corrosion (NACE [23])

Uniform Corrosion and Pitting Corrosion

After corrosion is initiated at the cracks, corrosion spreads across the surface of the piping between the outer pipe wall and the soil, where localized uniform corrosion and pitting corrosion have both been observed in water main piping. Both of these forms of corrosion are accelerated between the pipe walls and soil, where oxygen is depleted to create anodic surface areas near the cracks.

"Uniform corrosion is characterized by corrosive attack proceeding evenly over the entire surface area, or a large fraction of the total area. General thinning takes place until failure. If surface corrosion is permitted to continue, the surface may become rough and surface corrosion can lead to more serious types of corrosion" (NACE [22]).

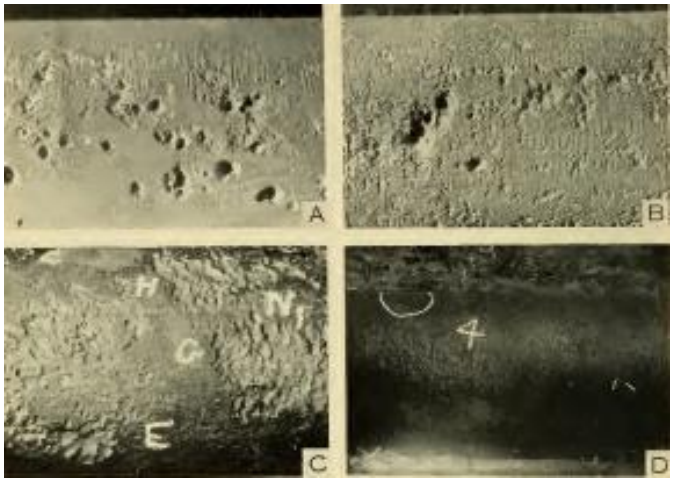

Figure 48: Uniform and Pitting Corrosion in Acidic Soils (Denison [24])

"Pitting corrosion is a localized form of corrosion by which cavities or "holes" are produced in the material. "Pitting is considered to be more dangerous than uniform corrosion damage because it is more difficult to detect, predict and design against. Corrosion products often cover the pits. A small, narrow pit with minimal overall metal loss can lead to the failure of an entire engineering system. Pitting corrosion, which, for example, is almost a common denominator of all types of localized corrosion attack, may assume different shapes. Pitting corrosion can produce pits with their mouth open (uncovered) or covered with a semi-permeable membrane of corrosion products. Pits can be either hemispherical or cup-shaped. Pitting may be initiated by localized chemical or mechanical damage to the protective oxide film; water chemistry factors which can cause breakdown of a passive film are acidity, low dissolved oxygen concentrations (which tend to render a protective oxide film less stable)". Also, brittle oxide coatings can be damaged due to impact during handling to initiate corrosion. This mechanism is possible, and the variable corrosion rates and potential moisture levels in soils would be consistent with failures discussed in the literature. "Theoretically, a local cell that leads to the initiation of a pit can be caused by an abnormal anodic site surrounded by normal surface which acts as a cathode, or by the presence of an abnormal cathodic site surrounded by a normal surface in which a pit will have disappeared due to corrosion" (NACE [23]) (See Fig. 47). When anodic sites are surrounded by cathodic

(acidic) soils, corrosion accelerates at localized points on pipe surfaces.

That is, uniform corrosion and pitting corrosion are expected to occur when water filters down from ground level to cause generalized corrosion over large sections of piping, rather than the observed corrosion conditions at only a few locations as observed in Figs. 5, 7, 10, and 14. This conclusion is based on research for underground piping, where piping was buried in acidic soils for 10 years and then excavated and examined. Corrosion results varied from pitted surfaces to uniform surfaces for similar pipes in different types of soils, as shown in (Fig. 48, Denison [24]). Again note that water hammers provide moisture sources to support corrosion.

WATER MAIN CORROSION SUMMARY

Engineering conclusions are stated here that significantly differ from previous engineering conclusions for water main corrosion failures. Consequently a clear and concise case is presented to support these conclusions, where the primary conclusion is that water hammer damage, accelerated by corrosion, is the primary cause of corrosion piping failures rather than corrosion itself as the primary cause of piping failure.

All of the conditions to explain water hammer induced piping corrosion failures lead from one to the other such that cracking due to water hammer → pipe leaks initiated → crevice corrosion influenced by galvanic corrosion → uniform and pitting corrosion caused by galvanic corrosion → leak rates increase → corrosion damage increases → pipes rupture into large leaks.

Note that underground metallic pipes are protected on the inside with concrete liners, e.g., ductile iron piping has a liner thickness of 1/16 inch for 3–12 inch diameter piping and3/32 inch for 14-24 inch diameter piping [25]. Also note that the maximum hoop stresses due to water hammer occur on the inner surfaces of piping, where cracks in the liner and pipe wall do not necessarily need to occur at the same locations[3]. Also note that soil resistivity to cause corrosion varies depending on geology, and may even vary locally at different locations, depending on the soil chemistry.

All in all, water hammer explains all of the observed conditions for corrosion failures - corrosion theory alone does not. Characteristics of failures were compared, and corrosion fails to meet all of the necessary criteria to support a conclusion that corrosion alone is the cause of water main piping failures. However, considerations of all of the observed conditions support an engineering judgement that water hammer cracks, accelerated by corrosion, are the cause of most, if not all, water main corrosion piping failures.

SUMMARY OF WATER HAMMER FATIGUE FAILURES

In short, the onslaught of piping failures for steel, ductile iron, HDPE, and other piping can be stopped, where these failures would not have occurred in the first place if water hammers were not intrinsic to pipe system operations. This new theory is consistent with observations that smaller diameter pipes are more likely to fail than larger diameter pipes, and more failures occur with age. When system failures occur due to large leaks in water main systems, the causes of pressure transients can be determined and corrected through the use of slow valve closures or variable frequency drives on pumps. Alternatively, this new theory can be used to prevent piping failures before they occur.

Note that this theory is applicable to failures in many other industries, which were not investigated here. Also, the National Transportation Safety Board provides an extensive history of cracked piping that transports petroleum and natural gas products throughout the U.S.

CONCLUSIONS AND RECOMMENDATIONS

The research presented here represents a paradigm shift in the understanding of hundreds of thousands of piping failures worldwide (Leishear [27]), where water main failures were investigated as partial examples of the immense scope of this problem. The invention of this one-man theory significantly advances technology to explain the failure stresses that cause piping fatigue failures, which are caused by water hammer. Previous static stress theory concluded that piping would not fail due to water hammer, but proof of principle has been provided here to demonstrate that water hammer does, in fact, result in both pipe cracks and corrosion in underground piping. Perhaps the stresses in this original dynamic stress theory could be coined as “Leishear Stresses”, where the author invented the theory, derived descriptive equations, and experimentally proved those equations. In short, underground water mains crack during service regardless of piping material, corrosion occurs at these crack sites, and water hammer causes these cracks.

[3] This observation is important, since a significant hole due to corrosion may form, while the inner concrete layer may remain intact as a cover over the opening. When the pressure on this thin covering sufficiently increases due to a corrosive increase in hole sizes, holes may suddenly blow out into substantial leaks. Note that experimental evidence is yet required with respect to this potential failure mechanism of the liner. Also note that many underground leaks may, or may not, reach the ground surface, where leaks can percolate to the surface in a matter of hours and then carve out a substantial flow path, since flow rates in soils vary between 0.05 and 10 inches per hour (Ref. [26]).

Further work in this area is warranted to investigate water main and other piping failures in light of this ground breaking new research. In short, a path to successful pipe failure analyses has been hammered into place for future research.

REFERENCES

[1] Leishear, R. A., 2013, *"Fluid Mechanics, Water Hammer, Dynamic Stresses, and Piping Design"*, ASME Press, American Society of Mechanical Engineers, New York, New York.

[2] Leishear, R. A., 2015, *"Supplement to Fluid Mechanics, Water Hammer, Dynamic Stresses, and Piping Design"*, ASME Press, American Society of Mechanical Engineers, New York, New York.

[3] NTSB, 2002, "NTSB Determines Probable Cause of Pipe Line Rupture in Bellingham Washington, National Transportation Safety Board, Washington, D.C.

[4] NTSB, 1974, "NTSB Safety Recommendations, Anhydrous Ammonia Pipeline Accidents, P-74-28", National Transportation Safety Board, Washington, D.C.

[5] Folkman, S., Rice, J., Sorrenson, A., Braithwaite, N., 2012, "Survey of Water Main Failures in the United States and Canada", Journal AWWA, American Water Works Association, Denver, Colorado.

[6] Water Services Association of Australia, 2003, "Common Failure Modes in Pressurized Pipeline Systems", Sydney, Australia.

[7] Rajeev, P., Kodikara, J., Robert D., Zeman P., and Rajani, B., 2013, "Factors Contributing to Large Diameter Water Pipe Failure as Evident From Failure Inspection", Monash University, Australia.

[8] Brooks and Choudry, 1993, "Metallurgical Failure Analysis," McGraw Hill Inc., New York, New York.

[9] Andersen, T., 1995, "Fracture Mechanics: Fundamentals and Applications", CRC Press, Boca Raton, Florida.

[10] Markl, A. R. C., 1952, "Fatigue Tests of Pipe Components," Transactions of the ASME, vol. 74, American Society of Mechanical Engineers, New York, pp. 287–303.

[11] Low, J. R., 1949, "Behavior of Metals under Direct or Nonreversing Loading, Properties of Metals in Engineering," American Society of Testing and Materials, Conshohocken, Pennsylvania.

[12] DIS, 2017, "Ductile Iron Data for Design Engineers", Ductile Iron Society, Strongsville, Ohio, www.ductile.org/didata/Section3.

[13] Khelif, R., Chateauneuf, A., Chaoui, K., 2008, "Statistical Analysis of HDPE Fatigue Lifetime", Meccanica, Springer Verlag, Berlin, Germany.

[14] Collins, J. A., 1993, "Failure of Materials in Mechanical Design", John Wiley and Sons, New York, New York.

[15] Green, D. J., 1993, "Technical Evaluation: 300 Area Steam Line Valve Accident, WHC-EP-0667," Westinghouse Hanford Company, Richland, Washington.

[16] AWWA, 2002, "ANSI/AWWA C151/A21.51-02, American National Standard for Ductile Iron Pipe, Centrifugally Cast, for Water", Denver, Colorado.

[17] "ASME B31.3, Process Piping," 2008, American Society of Mechanical Engineers, New York, New York. McGraw Hill, New York, New York.

[18] ASTM, "Standard Specification for Polyethylene (PE) Plastic Pipe (DR-PR) Based on Controlled Outside Diameter, D3035 − 14a", West Conshohocken, PA.

[19] ASTM, D3350 – 14, "Standard Specification for Polyethylene Plastics Pipe and Fittings Materials", West Conshohocken, Pennsylvania.

[20] NACE, 2018, "Galvanic Corrosion", National Association of Corrosion Engineers, www.nace.org/Corrosion-Central/Corrosion-101/Galvanic-Corrosion.

[21] NACE, 2018, "Crevice Corrosion", National Association of Corrosion Engineers, www.nace.org/Corrosion-Central/Corrosion-101/Crevice-Corrosion.

[22] NACE, 2018, "Uniform Corrosion", National Association of Corrosion Engineers, www.nace.org/Corrosion-Central/Corrosion-101/Uniform-Corrosion.

[23] NACE, 2018, "Pitting Corrosion", National Association of Corrosion Engineers, www.nace.org/Pitting-Corrosion.

[24] Denison, I., Hobbs, R., 1934 "Corrosion of Metal in Acid Soils", National Bureau of Standards, Gaithersburg, Maryland.

[25] "American National Standard for Cement-Mortar Lining for Ductile Iron Pipe and Fittings for Water", American Water Works Associations, Denver, Colorado.

[26] Plant and Sciences elibrary, 2018, Physical Properties of Soil and Water", https://passel.unl.edu/pages/informationmodule.php?idinformationmodule=1130447039&topicorder=10&maxto=10.

[27] Leishear, R., 2018, "Water Main Failures – A Billion Dollar a Year Problem", Empowering Pumps eMagazine.